ΛNN input to neutron stars from hypernuclear data

E. Friedman[a,*] and A. Gal[a]

[a]*Racah Institute of Physics,*
Hebrew University, Jerusalem 9190400, Israel

E-mail: eliahu.friedman@mail.huji.ac.il, avraham.gal@mail.huji.ac.il

This work is a sequel to our two 2023 publications [PLB 837 137669, NPA 1039 122725] where fitting 14 $1s_\Lambda$ and $1p_\Lambda$ single-particle binding energies in hypernuclei across the periodic table led to a well-defined Λ-nucleus optical potential. The potential consists of a Pauli modified linear-density (ΛN) and a quadratic-density (ΛNN) terms. The present work reports on extending the above analysis to 21 Λ single-particle data points input by including $1d_\Lambda$ and $1f_\Lambda$ states in medium-weight and heavy hypernuclei. The upgraded results for the ΛN and ΛNN potential depths at nuclear-matter density $\rho_0 = 0.17\,\mathrm{fm}^{-3}$, $D_\Lambda^{(2)} = -37.5 \mp 0.7$ MeV and $D_\Lambda^{(3)} = +9.8 \pm 1.2$ MeV together with the total depth $D_\Lambda = -27.7 \pm 0.5$ MeV, agree within errors with the earlier results. The Λ hypernuclear overbinding associated with the ΛN-induced potential depth $D_\Lambda^{(2)}$ agrees quantitatively with a recent combined analysis of low-energy Λp scattering data and correlation functions [PLB 850 (2024) 138550]. These results, particularly the size of the repulsive $D_\Lambda^{(3)}$, provide an essential input towards resolving the 'hyperon puzzle' in the core of neutron stars. We also show that a key property of our ΛNN-induced potential term, i.e. a need to suppress the quadratic-density ΛNN term involving an excess neutron and a nucleon in the $N = Z$ core, can be tested in the forthcoming JLab E12-15-008 experiment.

---

[*]*Speaker*

1. Introduction

Binding energies of Λ hyperons in single-particle states of Λ hypernuclei along the periodic table have been studied since the 1970s [1]. Although these data are fitted by several versions of optical-model and Skyrme-Hartree-Fock (SHF) approaches that differ in their high powers of the nuclear density ρ, the need to consider high powers of ρ has not been demonstrated unambiguously. Recent observations of neutron stars (NS) with mass exceeding twice solar mass are in conflict with the expectation that Λ hyperons in NS cores would soften the NS equation of state, thus preventing NS masses from exceeding ~ 1.5 solar mass. However, a mechanism of inhibiting the appearance of Λ hyperons through a repulsive ΛNN interaction apparently explains the astrophysical observations [2].

The present work offers a brief summary and an extension of our recent work [3, 4] on this topic. Using a simple density-dependent optical potential scheme, we check whether a *repulsive* ΛNN term is required by fits to the binding-energy data. In Sect. 2 the Λ optical potential is described focussing on nuclear densities based on nuclear sizes. Section 3.1 shows optical-potential predictions obtained by fitting $1s_\Lambda$ and $1p_\Lambda$ binding energies in $^{16}_{\Lambda}$N and then extrapolating the potential to heavier species. A need to suppress the ΛNN term when one nucleon is in the charge-symmetric core and the other is an 'excess' neutron is established, apparently related to its isospin dependence. Section 3.2 shows χ^2 fits to the full data set, including $1d_\Lambda$ and $1f_\Lambda$ states not shown yet. Section 3.3 demonstrates a way to study the isospin dependence of the ΛNN term in ^{40,48}Ca$(e, e'K^+)^{40,48}_{\Lambda}$K electroproduction experiments. And the last section presents comparisons with several interaction models in which the ΛN interaction overbinds Λ hypernuclei, thereby implying that the corresponding ΛNN contribution is indeed *repulsive*.

2. Methodology

The Λ-nuclear optical potential employed recently in our 2023 works [3, 4] is of the form $V_\Lambda^{\text{OPT}}(\rho) = V_\Lambda^{(2)}(\rho) + V_\Lambda^{(3)}(\rho)$, representing a two-body ΛN interaction

$$V_\Lambda^{(2)}(\rho) = -\frac{4\pi}{2\mu_\Lambda} \frac{f_A^{(2)} b_0}{1 + \frac{3k_F}{2\pi} f_A^{(2)} b_0} \rho \tag{1}$$

and three-body ΛNN interaction

$$V_\Lambda^{(3)}(\rho) = +\frac{4\pi}{2\mu_\Lambda} f_A^{(3)} B_0 \frac{\rho^2}{\rho_0}, \tag{2}$$

with b_0 and B_0 strength parameters in units of fm ($\hbar = c = 1$). In these expressions, μ_Λ is the Λ-nucleus reduced mass, ρ is nuclear density normalized to the mass number A of the nuclear core, $\rho_0 = 0.17$ fm^{-3} stands for nuclear-matter density and $f_A^{(2,3)}$ are kinematical factors involved in going from the ΛN and ΛNN c.m. systems, respectively, to the Λ-nucleus c.m. system [5]:

$$f_A^{(2)} = 1 + \frac{A-1}{A} \frac{\mu_\Lambda}{m_N}, \quad f_A^{(3)} = 1 + \frac{A-2}{A} \frac{\mu_\Lambda}{2m_N}. \tag{3}$$

The novelty of this presentation is connected to including explicitly Pauli correlations through the dependence of $V^{(2)}$ on the Fermi momentum $k_F = (3\pi^2\rho/2)^{1/3}$ which affects strongly the balance between the derived values of potential depths $D_\Lambda^{(2)}$ and $D_\Lambda^{(3)}$. This form for including Pauli correlations was suggested in Ref. [6] and practised in K^- atoms studies [7]. It is missing in most of SHF studies. We remark that the ΛNN potential term $V_\Lambda^{(3)}(\rho)$ derives mostly from OPE diagrams with ΣNN and $\Sigma^* NN$ intermediate states [8]. Purely ΛNN contributions are generated by NN short-range correlations [6], estimated in the present context to affect the derived value of $D_\Lambda^{(3)}$ by few percents at most. Finally, we note that the low-density limit of V_Λ^{OPT} requires that b_0 is identified with the c.m. ΛN spin-averaged scattering length [5], taken positive here.

In optical-model applications similar to the one adopted here it is crucial to ensure that the radial extent of the densities, e.g., their r.m.s. radii, follow closely values derived from experiment. With $\rho(r) = \rho_p(r) + \rho_n(r)$, the sum of proton and neutron density distributions, respectively, we relate the proton densities to the corresponding charge densities where the finite size of the proton charge and recoil effects are included. This approach is equivalent to assigning some finite range to the Λ-nucleon interaction. For the lightest elements in the database, harmonic-oscillator type densities were used for protons, assuming that the same radial parameters apply also for the corresponding neutron densities. For species beyond the nuclear $1p$ shell we chose two-parameter or three-parameter Fermi distributions normalized to Z for protons and $N = A - Z$ for neutrons, derived from nuclear charge distributions assembled in Ref. [9]. For medium-weight and heavy nuclei, the r.m.s. radii of neutron density distributions assume larger values than those for proton density distributions, as practised in analyses of exotic atoms [5]. Once neutrons occupy single-nucleon orbits beyond those occupied by protons, it is useful to represent the nuclear density $\rho(r)$ by

$$\rho(r) = \rho_{\mathrm{core}}(r) + \rho_{\mathrm{excess}}(r), \tag{4}$$

where ρ_{core} refers to the Z protons plus the charge-symmetric Z neutrons occupying the same nuclear 'core' orbits, and ρ_{excess} refers to the $(N - Z)$ 'excess' neutrons.

3. Results

3.1 Extrapolations from $^{16}_{\Lambda}\mathrm{N}$

As a preliminary test of the optical-model approach we chose to fit the binding energies of $1s_\Lambda$ and $1p_\Lambda$ states in the hypernucleus $^{16}_{\Lambda}\mathrm{N}$ because the simple $1p$ proton-hole structure of the $^{15}\mathrm{N}$ nuclear core removes, in this case, some of the uncertainty from spin-dependent ΛN and ΛNN interactions. $1s_\Lambda$ and $1p_\Lambda$ binding energies in Λ hypernuclei, deduced from several strangeness production reactions, are listed in Table IV of Ref. [1] including experimental uncertainties, and summarized in Table 2 of Ref. [4].

The top part of Fig. 1 (model X) shows comparisons with experiment when the parameters b_0 and B_0 of Eqs. (1,2), determined by a fit to the two binding energies in $^{16}_{\Lambda}\mathrm{N}$, are used to *predict* $1s_\Lambda$ and $1p_\Lambda$ binding energies along the periodic table. Clearly seen is underbinding of $1s_\Lambda$ and $1p_\Lambda$ states in the heavier hypernuclei, argued [3, 4] to result from
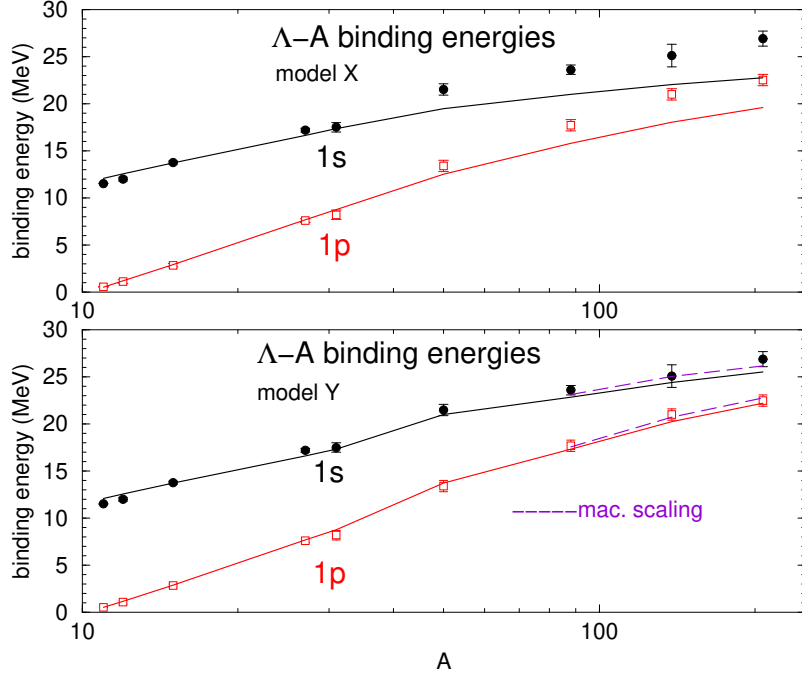
Figure 1: $B_\Lambda^{1s,1p}(A)$ values across the periodic table as calculated in models X (upper) and Y (lower), compared with data points, including uncertainties. Continuous lines connect calculated values. Figure updating Fig. 3 in Ref. [3]. The upper part, model X, uses the full ρ^2 term. The lower part, model Y, replaces ρ^2 by a reduced form, decoupling (N−Z) excess neutrons from $2Z$ symmetric-core nucleons, see text. The dashed lines are for ρ^2 replaced by $F\rho^2$, with a suppression factor F given by Eq. (6) below.

treating equally all NN pairs, including pairs where one nucleon is in the nuclear 'core' while the other is an 'excess' neutron. Removing the bilinear term from ρ^2 using Eq. (4) we replace ρ^2 for heavy species by

$$\rho_{\text{core}}^2 + \rho_{\text{excess}}^2 \rightarrow (2\rho_p)^2 + (\rho_n - \rho_p)^2, \tag{5}$$

in terms of the available densities ρ_p and ρ_n. This prescription follows from the $\vec{\tau}_1 \cdot \vec{\tau}_2$ isospin dependence arising from intermediate Σ and Σ^* hyperons in the ΛNN OPE interaction [8]. The reduced repulsion by the ΛNN term is seen in the lower part of Fig. 1 (model Y).

In the spirit of the present approach of avoiding explicit models, one can simply multiply ρ^2 by a suppression factor

$$F = \frac{(2Z)^2 + (N-Z)^2}{A^2}, \tag{6}$$

that is approximately the ratio of the volume integral of $(2\rho_p)^2 + (\rho_n - \rho_p)^2$ to that of ρ^2. This ratio is significant, going down to $F{=}0.67$ for Pb. Also seen in the figure as dashed lines ('mac. scaling') are results using $F\rho^2$ instead of Eq. (5), leading to almost identical results for the two options. It is interesting that extrapolating from $^{16}_{\Lambda}$N to $^{208}_{\Lambda}$Pb is successful in describing the experimental results, while going down from $^{16}_{\Lambda}$N into the nuclear p-shell (two smallest A-values) does not support the present simple model.

3.2 Least-squares fits

Next we performed conventional χ^2 fits with the suppression factor F included for the four heaviest species. Figure 2 shows several fits to the B_Λ data where black solid lines show fits to the full data set and open circles with error bars mark B_Λ data points. It is clearly seen that the $1s_\Lambda$ states in $^{12}_\Lambda$B and $^{13}_\Lambda$C do not fit into the otherwise good agreement with experiment for the heavier species. The red dashed lines show a very good fit obtained upon excluding these light elements from the B_Λ data set. In fact, the potential parameters b_0 and B_0 of Eqs. (1,2) are hardly affected by the two lightest $^{12}_\Lambda$B and $^{13}_\Lambda$C hypernuclei. The fit parameters are:

$b_0 = 1.44 \pm 0.095$ fm (attraction), $B_0 = 0.190 \pm 0.024$ fm (repulsion),

with 100% correlation between the two parameters. The fully correlated partial potential depths and the full one at nuclear-matter density $\rho_0 = 0.17$ fm^{-3} are (in MeV):

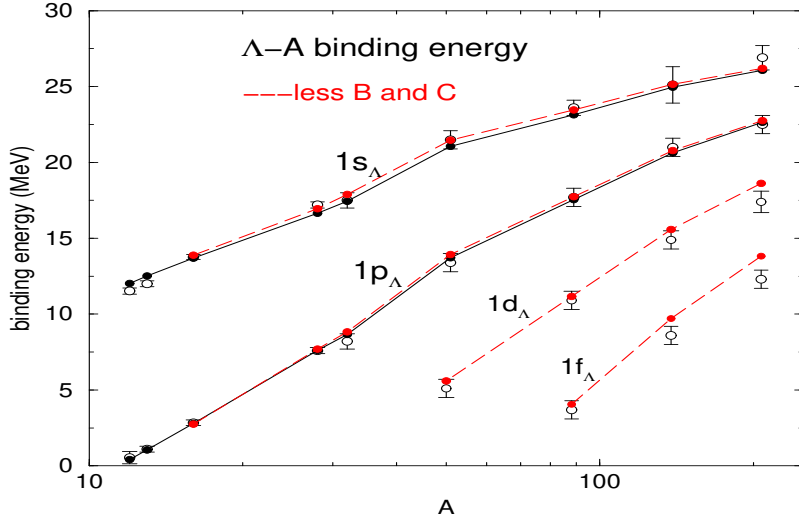$$D_\Lambda^{(2)} = -38.6 \mp 0.8, \quad D_\Lambda^{(3)} = 11.3 \pm 1.4, \quad D_\Lambda = -27.3 \pm 0.6. \tag{7}$$

Figure 2: χ^2 fits to the full $1s_\Lambda$ and $1p_\Lambda$ data (solid black lines) and when excluding $^{12}_\Lambda$B and $^{13}_\Lambda$C (dashed red lines). Also shown are *predictions* of $1d_\Lambda$ and $1f_\Lambda$ binding energies for the latter choice.

Also included in Fig. 2 are *predictions* of $1d_\Lambda$ and $1f_\Lambda$ binding energies made with these parameters. Although it is not expected that higher states will be well described by the same potential, owing to overlooked secondary effects such as non-local terms, it is seen that while slight overbinding of the calculated energies appears for the heavier species, the present optical potential reproduces quite well the four deepest Λ single-particle states in neutron-rich hypernuclei. It is therefore of interest to repeat the χ^2 process on the whole set of experimental binding energies of Λ single-particle states, a total of 21 binding-energy values between $^{16}_\Lambda$N and $^{208}_\Lambda$Pb. The resulting χ^2 per degree of freedom is then 0.95 (compared to 0.6 from a fit to only 14 binding-energy values for the $1s_\Lambda$ and $1p_\Lambda$ states)

and the potential parameters are:

$b_0 = 1.32 \pm 0.072$ fm (attraction), $B_0 = 0.162 \pm 0.020$ fm (repulsion),

with 100% correlation between the two parameters. The fully correlated partial potential depths and the full one at nuclear-matter density $\rho_0 = 0.17$ fm^{-3} are (in MeV):

$$D_\Lambda^{(2)} = -37.5 \mp 0.7, \quad D_\Lambda^{(3)} = 9.8 \pm 1.2, \quad D_\Lambda = -27.7 \pm 0.5. \tag{8}$$

These values are in agreement with those in Eq. (7) based only on $1s_\Lambda$ and $1p_\Lambda$ states. The uncertainties in the parameter values quoted above are statistical only. To estimate systematic effects within the adopted model we repeated the analysis with slightly modified nuclear densities such as obtained when unfolding the finite size of the proton. Values of b_0 came out unchanged whereas values of B_0 increased typically by 0.015 fm. The total potential depth at $\rho_0 = 0.17$ fm^{-3} changed to $D_\Lambda = -26.9 \pm 0.4$ MeV, suggesting a systematic uncertainty of 1 MeV for this value.

3.3 Isospin dependence

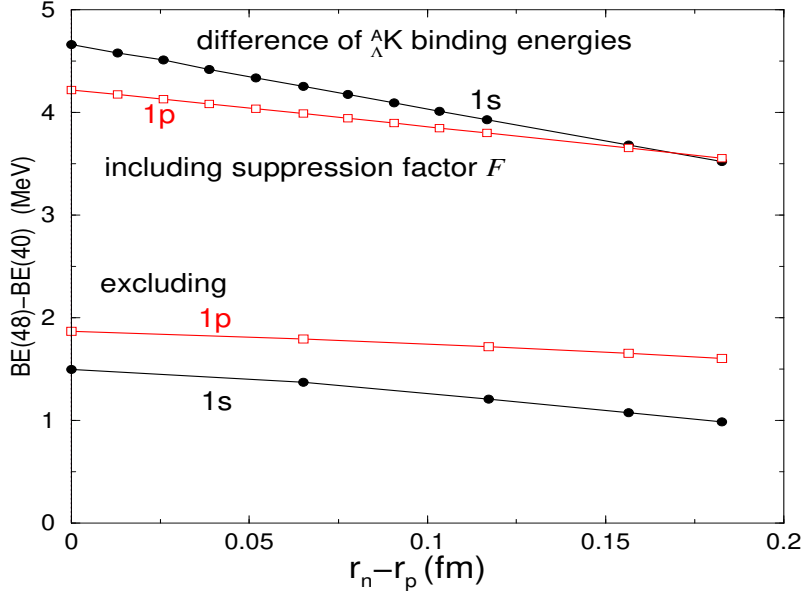**Figure 3:** $B_\Lambda(^{48}_\Lambda\text{K}) - B_\Lambda(^{40}_\Lambda\text{K})$ values for $1s_\Lambda$ and $1p_\Lambda$ states, with and without applying the suppression factor F, as a function of the neutron-skin of $^{48}_\Lambda\text{K}$, see text.

Figure 3 shows calculated differences of Λ binding energies for the $1s_\Lambda$ and $1p_\Lambda$ states between $^{48}_\Lambda\text{K}$ and $^{40}_\Lambda\text{K}$ as a function of the neutron skin $r_n - r_p$ in $^{48}_\Lambda\text{K}$. The figure shows predictions made using our standard Λ-nucleus potential V_Λ^{OPT} upon including (excluding) in its upper (lower) part the suppression factor F, Eq. (6). Regardless of the chosen value of $r_n - r_p$, the effect of applying F is about 2.5 MeV for the $1s_\Lambda$ state and more than 2 MeV for the $1p_\Lambda$ state, within reach of the $(e, e'K^+)$ approved JLab experiment E12-15-008 on ^{40,48}Ca targets [10]. For $F = 1$, our calculated B_Λ values are close to those calculated in Refs. [11, 12].

Model	$D_\Lambda^{(2)}$	$D_\Lambda^{(3)}$	D_Λ
Nijmegen ESC16,16$^+$ [16]	-43.7	$+5.8$	-37.9
EFT NLO19 [17]	-39 to -29	$-$	$-$
NLO19 + **10** dominance [2, 18]	≈ -36	$\approx +10$	
EFT N^{2}LO [19]	-33 to -38	$-$	$-$
Femtoscopy [20]	$-36.3 \pm 1.3(\text{stat.})^{+2.5}_{-6.2}(\text{syst.})$	$-$	$-$
Hypernuclear constraints (present)	-37.5 ∓ 0.7	9.8 ± 1.2	-27.7 ± 0.5

Table 1: Two-body, three-body and total Λ-nucleus potential depths (in MeV) at nuclear matter density $\rho_0 = 0.17\,\text{fm}^{-3}$ from several *model* calculations and from hypernuclear binding-energy data.

4. Discussion and summary

The most significant results of the present phenomenological analysis using the $V_\Lambda^{\text{OPT}}(\rho)$ methodology are the values at nuclear matter density of the two-body and three-body potentials, namely the partial depths $D_\Lambda^{(2)}$ and $D_\Lambda^{(3)}$ as well as their sum D_Λ listed in Eq. (8). Microscopic models employed in calculations of astrophysical scenarios could then be tested for the first time in normal nuclear matter by comparing to the present results. SHF models, in contrast, do not produce reliable values of $D_\Lambda^{(2)}$ and $D_\Lambda^{(3)}$. This holds for both old [13] as well as recent [14, 15] SHF calculations.

Table 1 shows comparisons between several recent *model* predictions and the *present* results for Λ-nuclear potential depths. Note that *all* model values of $D_\Lambda^{(2)}$ are overbound with respect to the empirical depth value of $D_\Lambda \approx -30$ MeV from Λ hypernuclei [1] which tacitly enters such model calculations. In comparison with our listed value of D_Λ, this overbinding suggests a *repulsive* ΛNN contribution of depth $D_\Lambda^{(3)} \approx 10$ MeV, a value indeed reached by one of the EFT model calculations [18] and in agreement with our listed value. It would be interesting to repeat this model calculation using our value of $D_\Lambda = -27.7 \pm 0.5$ MeV as input. The bottom line of this NLO19 EFT plus baryon decuplet (**10**) dominance model calculation is that hyperons are excluded from dense neutron stars owing to a ΛNN term of a strength commensurate with $D_\Lambda^{(3)} \approx 10$ MeV.

References

[1] A. Gal, E.V. Hungerford, D.J. Millener, *Strangeness in nuclear physics,* Rev. Mod. Phys. 88 (2016) 035004.

[2] D. Gerstung, N. Kaiser, W. Weise, *Hyperon-nucleon three-body forces and strangeness in neutron stars,* Eur. Phys. J. A 56 (2020) 175.

[3] E. Friedman, A. Gal, *Constraints from Λ hypernuclei on the ΛNN content of the Λ nucleus potential,* Phys. Lett. B 837 (2023) 137669.

[4] E. Friedman, A. Gal, *Λ hypernuclear potentials beyond linear density dependence,* Nucl. Phys. A 1039 (2023) 122725.

[5] E. Friedman, A. Gal, *In-medium nuclear interactions of low-energy hadrons,* Phys. Rep. 452 (2007) 89.

[6] T. Waas, M. Rho, W. Weise, *Effective kaon mass in dense baryonic matter: role of correlations,* Nucl. Phys. A 617 (1997) 449.

[7] E. Friedman, A. Gal, $K^- N$ *amplitudes below threshold constrained by multinucleon absorption,* Nucl. Phys. A 959 (2017) 66.

[8] A. Gal, J.M. Soper, R.H. Dalitz, *A shell-model analysis of Λ binding energies, I,* Ann. Phys. (NY) 63 (1971) 53.

[9] I. Angeli, K.P. Marinova, *Table of experimental nuclear ground state charge radii: An update,* At. Data Nucl. Data Tables 99 (2013) 69.

[10] S.N. Nakamura, *Future prospects of spectroscopic study of Λ hypernuclei at JLab,* EPJ Web of Conf. 271 (2022) 11003.

[11] M. Isaka, Y. Yamamoto, Th.A. Rijken, *Effects of a hyperonic many-body force on $B_Λ$ values of hypernuclei,* Phys. Rev. C 95 (2017) 044308.

[12] P. Bydžovsky, et al., *Self-consistent many-body approach to the electroproduction of hypernuclei,* Phys. Rev. C 108 (2023) 024615.

[13] D.J. Millener, C.B. Dover, A. Gal, *Λ-nucleus single-particle potentials,* Phys. Rev. C 38 (1988) 2700.

[14] H.-J. Schulze, E. Hiyama, *Skyrme force for light and heavy hypernuclei,* Phys. Rev. C 90 (2014) 047301.

[15] A. Jinno, K. Murase, Y. Nara, A. Ohnishi, *Repulsive Λ potentials in dense neutron star matter and binding energy of Λ in hypernuclei,* Phys. Rev. C 108 (2023) 065803.

[16] M.M. Nagels, Th.A. Rijken, Y. Yamamoto, *Extended-soft-core baryon-baryon model ESC16. II. YN interactions,* Phys. Rev. C 99 (2019) 044003.

[17] J. Haidenbauer, U.-G. Meißner, A. Nogga, *Hyperon-nucleon interaction within χEFT revisited,* Eur. Phys. J. A 56 (2020) 91.

[18] W. Weise, *Sound velocity, equation of state and strangeness in neutron star matter,* EPJ Web of Conf. 291 (2024) 01007.

[19] J. Haidenbauer, U.-G. Meißner, A. Nogga, H. Le, *Hyperon-nucleon interaction in χEFT at N^2LO,* Eur. Phys. J. A 59 (2023) 63.

[20] D.L. Mihaylov, J. Haidenbauer, V. Mantovani Sarti, *Constraining the pΛ interaction from a combined analysis of scattering data and correlation functions,* Phys. Lett. B 850 (2024) 138550.